MLCK-dependent exchange and actin binding region-dependent anchoring of ZO-1 regulate tight junction barrier function

Dan Yu, Amanda M. Marchiando[1], Christopher R. Weber[1], David R. Raleigh, Yingmin Wang, Le Shen[2], and Jerrold R. Turner[2]

Department of Pathology, The University of Chicago, Chicago, IL 60637

Edited by W. James Nelson, Stanford University School of Medicine, Stanford, CA, and accepted by the Editorial Board March 26, 2010 (received for review August 5, 2009)

The perijunctional actomyosin ring contributes to myosin light chain kinase (MLCK)-dependent tight junction regulation. However, the specific protein interactions involved in this process are unknown. To test the hypothesis that molecular remodeling contributes to barrier regulation, tight junction protein dynamic behavior was assessed by fluorescence recovery after photobleaching (FRAP). MLCK inhibition increased barrier function and stabilized ZO-1 at the tight junction but did not affect claudin-1, occludin, or actin exchange in vitro. Pharmacologic MLCK inhibition also blocked in vivo ZO-1 exchange in wild-type, but not long MLCK$^{-/-}$, mice. Conversely, ZO-1 exchange was accelerated in transgenic mice expressing constitutively active MLCK. In vitro, ZO-1 lacking the actin binding region (ABR) was not stabilized by MLCK inhibition, either in the presence or absence of endogenous ZO-1. Moreover, the free ABR interfered with full-length ZO-1 exchange and reduced basal barrier function. The free ABR also prevented increases in barrier function following MLCK inhibition in a manner that required endogenous ZO-1 expression. In silico modeling of the FRAP data suggests that tight junction-associated ZO-1 exists in three pools, two of which exchange with cytosolic ZO-1. Transport of the ABR-anchored exchangeable pool is regulated by MLCK. These data demonstrate a critical role for the ZO-1 ABR in barrier function and suggest that MLCK-dependent ZO-1 exchange is essential to this mechanism of barrier regulation.

fluorescence recovery after photobleaching | mathematical models | myosin light chain kinase | paracellular permeability | intestinal epithelium

Great progress has been made toward identifying components of the tight junction. These include transmembrane, peripheral membrane, and regulatory proteins, many of which contain one or more domains that mediate interactions with other tight junction and cytoskeletal proteins (1). These and other observations drove development of models that depicted the tight junction as a static, heavily cross-linked protein complex (2). However, recent data showing rapid and continuous remodeling of the tight junction refuted the previous models and led to the hypothesis that modulation of protein remodeling behavior could be a mechanism of tight junction barrier regulation (3, 4).

The perijunctional ring of F-actin and myosin II that supports the tight junction is essential to physiological and pathophysiological barrier regulation (5). For example, activation of perijunctional myosin light chain kinase (MLCK) is sufficient to enhance paracellular permeability (6, 7) and is required for tight junction barrier regulation in response to Na^+-nutrient cotransport, inflammatory cytokines, or pathogenic bacteria (8). Thus, modulation of MLCK activity represents a point of convergence for multiple signaling pathways that regulate tight junction barrier function.

To assess the role of molecular remodeling in barrier regulation, dynamic behaviors of tight junction proteins were assessed before and after MLCK inhibition. Zonula occludens 1 (ZO-1), but not claudin-1, occludin, or actin, was stabilized at the tight junction following MLCK inhibition. This stabilization required the actin binding region (ABR), a 220-amino-acid domain within the carboxyl-terminal half of ZO-1 (9). Moreover, when expressed as an EGFP-fusion protein, the ABR interfered with ZO-1 exchange and prevented both ZO-1 stabilization and barrier regulation following MLCK inhibition. The data indicate that tight junction-associated ZO-1 is the sum of three pools, two of which exchange with the cytosolic pool by distinct mechanisms. The data also suggest that MLCK- and ABR-dependent ZO-1 exchange and anchoring, respectively, are critical determinants of tight junction barrier function.

Results

MLCK-Dependent Barrier Regulation Is Associated with ZO-1 Stabilization at the Tight Junction. Validated fluorescent fusion constructs of claudin-1, occludin, and ZO-1 were expressed in Caco-2 cells with active Na^+-glucose cotransport (10, 11), a model in which MLCK-dependent tight junction regulation has been extensively characterized. Fluorescence recovery after photobleaching (FRAP) studies (Fig. 1 *A* and *B*) demonstrated that these proteins exchanged with kinetics similar to those observed in MDCK cells (3); a small decrease in ZO-1 mobile fraction (Table S1) was the most notable difference. Thus, overall tight junction protein dynamic behavior at steady state is similar in confluent Caco-2 and MDCK epithelial cell monolayers.

Monolayers were next treated with PIK, a highly-specific peptide inhibitor of MLCK (12), which induced a 46% ± 5% increase in transepithelial electrical resistance (TER) and reduced the ZO-1 mobile fraction, i.e., the fraction of total tight junction-associated full-length ZO-1 available for exchange, from 56 ± 3 to 20 ± 5% (Fig. 1 *B* and *C* and Fig. S1 *D–F*). PIK also reduced the $t_{1/2}$ of ZO-1 FRAP from 125 ± 8 s to 39 ± 11 s (Fig. 1*B* and Table S2). In contrast, PIK did not affect the dynamic behaviors of claudin-1, occludin, or actin (Fig. 1 *A* and *B*). These data suggest that MLCK activity is critical to ZO-1 (but not claudin-1, occludin, or actin) exchange at the tight junction.

ZO-1 Exchange Requires Actomyosin Function. To determine if the observed effects of MLCK inhibition on ZO-1 extended to other forms of cytoskeletally-mediated tight junction regulation,

Author contributions: D.Y., L.S., and J.R.T. designed research; D.Y., A.M.M., C.R.W., D.R.R., Y.W., L.S., and J.R.T. performed research; L.S. and J.R.T. contributed new reagents/analytic tools; D.Y., C.R.W., L.S., and J.R.T. analyzed data; and D.Y., L.S., and J.R.T. wrote the paper.

The authors declare no conflict of interest.

This article is a PNAS Direct Submission. W.N. is a guest editor invited by the Editorial Board.

Data deposition: The models used in this paper are accessible at the Virtual Cell web site vcell.org/vcell_models/published_models.html.

[1]A.M.M. and C.R.W. contributed equally to this work.

[2]To whom correspondence may be addressed. E-mail: jturner@bsd.uchicago.edu or leshen@uchicago.edu.

This article contains supporting information online at www.pnas.org/cgi/content/full/0908869107/DCSupplemental.

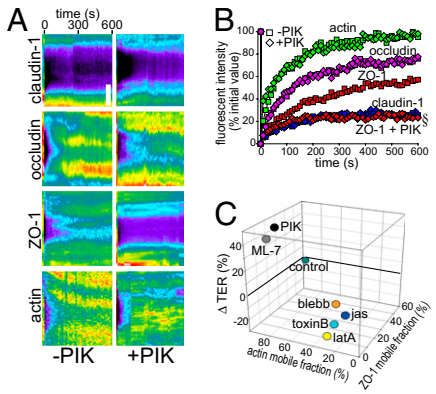

Fig. 1. MLCK inhibition uniquely stabilizes ZO-1 at the tight junction in vitro. (*A*) Caco-2 monolayers stably expressing fluorescent fusion constructs were studied by FRAP 15 min after addition of the specific MLCK inhibitor PIK (250 μM). (Scale bar, 3 μm.) (*B*) Mean recovery curves, $n = 4$ per condition. § $P < 0.001$ vs. ZO-1 without PIK. (*C*) TER and FRAP of ZO-1 and actin were assessed 15 min after addition of 0.5 μM latrunculin A (latA); 1 μM jasplakinolide (jas); 10 μM blebbistatin (blebb); 250 μM PIK; 10 μM ML-7; or 40 ng/mL toxin B, $n = 4$ per condition.

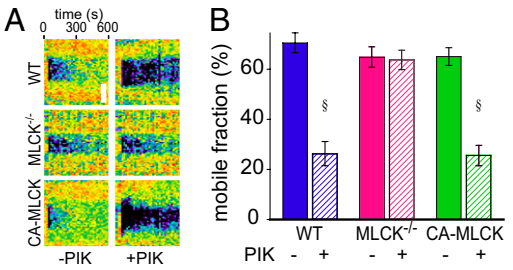

Fig. 2. MLCK regulates ZO-1 exchange in vivo. (*A*) mRFP1-ZO-1 FRAP was assessed in wild-type (WT), long MLCK$^{-/-}$, and CA-MLCK transgenic mice. PIK (250 μM) was added 15 min before analysis. (Scale bar, 3 μm.) (*B*) Mobile fraction of mRFP1-ZO-1, $n = 5$ per condition. § $P < 0.001$ vs. corresponding mucosa after PIK treatment.

monolayers were treated with agents that perturb either actin or myosin function. Latrunculin A was used to disrupt actin polymerization (13, 14), jasplakinolide to limit microfilament disassembly and enhance actin polymerization (15), blebbistatin to inhibit myosin II ATPase and disrupt cyclic actomyosin interactions (16, 17), and *Clostridium difficile* toxin B to inhibit rhoA (18). Each treatment interfered with perijunctional actin exchange, whereas PIK and the less specific MLCK inhibitor ML-7 did not affect actin FRAP (Fig. 1*C* and Fig. S1*I*). In contrast, all drugs significantly reduced ZO-1 exchange (Fig. 1*C* and Fig. S1*J*). The impact of these treatments on barrier function correlated perfectly with the FRAP effects; agents that inhibited only ZO-1 FRAP increased TER, whereas those that inhibited both ZO-1 and actin FRAP reduced TER (Fig. 1*C* and Fig. S1 *G*, *I*, and *J*). Importantly, all drugs were used at low concentrations and did not disrupt claudin-1, occludin, ZO-1, E-cadherin, or perijunctional actin (Fig. S1*H*). Thus, actomyosin function is important for both barrier maintenance and ZO-1 exchange.

ZO-1 Exchange Is Regulated via MLCK in Vivo. To determine if the in vitro data corresponded to in vivo behavior, FRAP was performed using transgenic mice expressing mRFP1-ZO-1 under control of the 9-kb villin promoter. These studies relied on a method that allows maintenance of the intestinal neurovascular supply during imaging (Fig. S2*A*). mRFP1-ZO-1 was correctly localized at tight junctions throughout the villus epithelium (Fig. S2*B*), and FRAP analyses showed that in vivo exchange occurred with a mobile fraction of 70% ± 5% (Fig. 2, and Fig. S2 and Table S3), slightly greater than that of Caco-2 monolayers. Similar to the in vitro result, in vivo pharmacological MLCK inhibition reduced both the ZO-1 mobile fraction (to 26% ± 4%) and $t_{1/2}$ (Fig. 2 and Tables S2 and S3).

Although PIK is highly specific for MLCK, the possibility that the observed ZO-1 stabilization represents off-target effects must be considered. To assess this, mRFP1-ZO-1 transgenic mice were bred with knockout mice that lack long MLCK, the isoform expressed in intestinal epithelia (19, 20). The ZO-1 mobile fraction and $t_{1/2}$ were not significantly different from those measured in wild-type mice (Fig. 2, Fig. S2, and Table S3). This suggests that, as is commonly observed in knockout mice, there has been compensation for the loss of long MLCK and is consistent with the normal basal jejunal barrier function and epithelial MLC phosphorylation reported in long MLCK$^{-/-}$ mice (19). Moreover, the MLCK inhibitor PIK did not affect ZO-1 FRAP behavior in MLCK$^{-/-}$ mice (Fig. 2, Fig. S2, and Table S3). Long MLCK is therefore required for reduced ZO-1 recovery after PIK treatment. Thus, the ZO-1 stabilization induced by PIK is due to MLCK inhibition rather than nonspecific drug effects.

To determine whether ZO-1 exchange is influenced by MLCK activation, mRFP1-ZO-1 transgenic mice were bred with transgenic mice that express constitutively active MLCK (CA-MLCK) under control of the 9-kb villin promoter (7). CA-MLCK expression did not affect the ZO-1 mobile fraction but significantly reduced the $t_{1/2}$ of recovery (Fig. 2, Fig. S2, and Table S3). ZO-1 exchange in CA-MLCK mice following PIK treatment (Fig. 2, Fig. S2, and Table S3) was similar to that in PIK-treated wild-type mice, consistent with the previously reported inhibition of CA-MLCK by PIK (6, 7). Thus, in vivo ZO-1 exchange is regulated by both MLCK activation and inhibition.

The ABR Is Required for ZO-1 Stabilization After MLCK Inhibition. ZO-1 association with actin is mediated, at least in part, by the ABR (9, 21). As the data above show that actomyosin function is required for ZO-1 exchange, we sought to determine if the ABR is involved in ZO-1 transport to or stabilization at the tight junction. An EGFP-tagged ZO-1 deletion mutant lacking the ABR (residues 1152–1371) was stably expressed in Caco-2 cells. EGFP-ZO-1$^{\Delta ABR}$ was efficiently targeted to the tight junction in confluent Caco-2 monolayers (Fig. S3*A*), and the distributions of claudin-1, occludin, endogenous ZO-1, E-cadherin, and actin were not grossly disturbed by EGFP-ZO-1$^{\Delta ABR}$ expression (Fig. S3*B*). However, EGFP-ZO-1$^{\Delta ABR}$ expression did increase monolayer TER (Fig. S4*A*). The reasons for this TER elevation are not clear, but may be secondary to limited decoupling of the tight junction and perijunctional actomyosin ring. This hypothesis is consistent with previous reports showing that treatment with low concentrations of cytochalasin D increases TER of MDCK and Caco-2 cell monolayers (10, 22, 23).

ABR deletion did not affect FRAP $t_{1/2}$, but the EGFP-ZO-1$^{\Delta ABR}$ mobile fraction (81% ± 5%) was significantly greater than that of full length EGFP-ZO-1 (Fig. 3*A* and Table S2). This suggests that the ABR plays a role in basal ZO-1 stabilization at the tight junction. Moreover, ZO-1$^{\Delta ABR}$ FRAP was not affected by MLCK inhibition with PIK or the less specific MLCK inhibitor ML-7 (Fig. 3*A* and Fig. S3*C*), suggesting that the ABR is necessary for increased ZO-1 stabilization after MLCK inhibition. EGFP-ZO-1$^{\Delta ABR}$ FRAP was similar in Caco-2 cells lacking endogenous ZO-1 (Fig. 3*B*), indicating that the results were not influenced by interactions between EGFP-ZO-1$^{\Delta ABR}$ and full-length ZO-1. Therefore, the ABR contributes to ZO-1 stabilization at the tight junction, both at steady state and in response to MLCK inhibition. Moreover, the observation that EGFP-ZO-1$^{\Delta ABR}$ FRAP was sensitive to latrunculin A, jasplakinolide, blebbistatin, and toxin B, despite resistance to PIK and ML-7, suggests the presence of a second mechanism of ZO-1

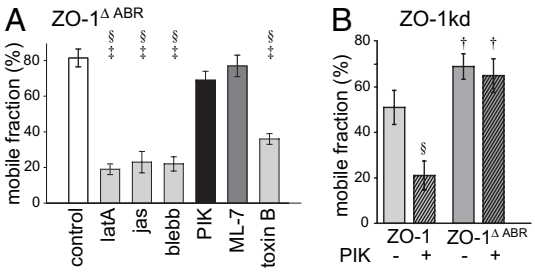

Fig. 3. The ABR is required for ZO-1 stabilization after MLCK inhibition. (*A*) EGFP-ZO-1$^{\Delta ABR}$ FRAP was assessed after addition of drugs, as in Fig. 1, and mobile fraction determined, $n = 4$ per condition. § $P < 0.001$ vs. untreated (control) monolayers. ‡ $P < 0.001$ vs. PIK-treated monolayers. (*B*) Mobile fraction of EGFP–ZO-1 or EGFP-ZO-1$^{\Delta ABR}$ expressed in ZO-1 knockdown (kd) monolayers, $n = 3$ per condition. † $P < 0.05$ vs. control ZO-1 expressing monolayers. § $P < 0.001$ vs. corresponding PIK-treated monolayers.

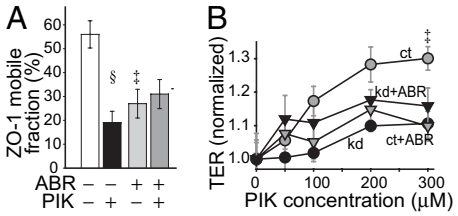

Fig. 4. ABR expression reduces barrier function and prevents TER increases after MLCK inhibition. (*A*) Mobile fraction of mRFP1–ZO-1 FRAP in monolayers also expressing EGFP-ZO-1 or EGFP-ABR, as indicated, without or with 250 μM PIK, $n = 3$. § $P < 0.001$ vs. monolayers without PIK. ‡ $P < 0.01$ vs. full-length EGFP-ZO-1-expressing monolayers. (*B*) PIK induces a dose-dependent increase in TER of control (ct) monolayers but not ZO-1 knockdown (kd) or EGFP-ABR-expressing monolayers, $n = 3$ per condition. ‡ $P < 0.01$ vs. all other conditions.

exchange that depends on global actomyosin function but does not require the ABR or MLCK activity.

Analysis of MDCK cells has shown that tight junction-associated ZO-1 exchanges with a cytosolic pool by a process that does not involve diffusion at the membrane (3). However, the data above raise the possibility that a component of EGFP-ZO-1$^{\Delta ABR}$ FRAP in Caco-2 cells may involve diffusion at the membrane, as occurs with occludin (3). To assess this, recovery of EGFP-ZO-1 and EGFP-ZO-1$^{\Delta ABR}$ FRAP was assessed over an extended region of the tight junction. As in MDCK cells (3), recovery was uniform over the entire area (Fig. S5 *A–C*). Moreover, both EGFP-ZO-1 and EGFP-ZO-1$^{\Delta ABR}$ FRAP were inhibited by ATP depletion but unaffected by reduced temperature, cholesterol depletion, or inhibition of small GTPase-regulated membrane traffic (Fig. S5 *D* and *E*). Thus, both MLCK-dependent and MLCK-independent mechanisms of ZO-1 and ZO-1$^{\Delta ABR}$ FRAP in Caco-2 cells involve ATP-dependent exchange with a cytosolic pool but not diffusion within the membrane.

Free ABR Expression Prevents ZO-1 Exchange and Tight Junction Barrier Regulation. The studies of ZO-1$^{\Delta ABR}$ suggest that ABR-mediated interactions are critical to ZO-1 stabilization. However, it is also possible that ABR deletion disrupts folding of the carboxyl-terminal portion of ZO-1 and, therefore, interferes with function of adjacent domains. To assess this possibility, EGFP-ABR, without other ZO-1 domains, was expressed in Caco-2 cells, where it was distributed at the junction as well as diffusely throughout the cytosol (Fig. S6). These cells, as well as those expressing EGFP-ZO-1, were transfected with mRFP1-ZO-1 to assess the effects of the ABR on FRAP behavior of full-length ZO-1. EGFP-ZO-1, EGFP-ZO-1$^{\Delta ABR}$, and mRFP1-ZO-1 were correctly delivered to the tight junction (Fig. S6).

FRAP analysis demonstrated that mRFP1-ZO-1 exchange in cells expressing EGFP-ZO-1 was identical to that of EGFP-ZO-1 in wild-type cells (Fig. 4 and Fig. S6), both before and after MLCK inhibition (Fig. 4 and Fig. S6). EGFP-ZO-1$^{\Delta ABR}$ slightly reduced the basal mobile fraction of mRFP1-ZO-1, but exchange was still sensitive to MLCK inhibition (Fig. S6). In contrast, EGFP-ABR markedly decreased the mRFP1-ZO-1 mobile fraction at steady-state (Fig. S6), and MLCK inhibition did not induce any further reduction of mRFP1-ZO-1 FRAP in EGFP-ABR-expressing cells (Fig. 4*A* and Fig. S6). These data suggest that free ABR disrupts ABR-dependent full-length ZO-1 interactions required for stabilization before and after MLCK inhibition but does not interfere with ZO-1 trafficking.

EGFP-ABR reduced TER in Caco-2 cells expressing endogenous ZO-1 but not in ZO-1 knockdown Caco-2 cells (Fig. S6*A*). These data suggest that the effect of EGFP-ABR expression on TER is secondary to inhibition of endogenous ZO-1 function, rather than nonspecific actomyosin disruption, and are consistent with the effect of EGFP-ABR on MLCK-dependent mRFP1-ZO-1 exchange (described above). To test the hypothesis that ABR-mediated interactions are also necessary for MLCK-dependent barrier regulation, the effect of PIK was assessed in control and ZO-1 knockdown Caco-2 monolayers in the presence and absence of EGFP-ABR expression. As reported previously (12), PIK caused a dose-dependent increase in TER of wild-type monolayers (Fig. 4*B*). In contrast, the effect of PIK on TER was small and dose-independent in ZO-1 knockdown monolayers (Fig. 4*B*), indicating that ZO-1 is required for MLCK-dependent tight junction barrier regulation. The TER response to MLCK inhibition was not affected by EGFP-ABR expression in ZO-1 knockdown monolayers (Fig. 4*B*). Most importantly, expression of EGFP-ABR in wild-type monolayers limited TER increases induced by MLCK inhibition to small, dose-independent responses that were indistinguishable from the responses of ZO-1 knockdown monolayers (Fig. 4*B*). These data demonstrate that MLCK-dependent tight junction barrier regulation requires ZO-1 and can be specifically disrupted by free ABR expression.

A Unified Model Can Simulate in Vitro and in Vivo ZO-1 FRAP Behavior. Steady-state ZO-1 FRAP in MDCK cells has been modeled as three pools; a fixed (nonexchangeable) tight junction pool, an exchangeable tight junction pool, and an exchangeable cytosolic pool (3). To better understand the regulation of ZO-1 exchange in Caco-2 cells, FRAP behavior was modeled in silico on the basis of known ZO-1 function and experimental data. The in vitro data show that exchange of tight junction-associated ZO-1 and ZO-1$^{\Delta ABR}$ in Caco-2 cells also occurs via ATP-dependent exchange with a cytosolic pool, rather than diffusion within the membrane (Fig. S5). The results further indicate that at least two mechanisms, one of which involves MLCK and the ABR, are involved in exchange of tight junction-associated and cytosolic ZO-1.

The two exchangeable pools of tight junction-associated ZO-1 were modeled as PIK-sensitive and PIK-insensitive FRAP components (Fig. 5). A fixed pool of tight junction-associated ZO-1 was also defined, with the remainder of total ZO-1 within a cytosolic pool. Diffusion within the cytosolic pool was modeled as occurring at a fixed rate (Table S4). Rate constants and pool size of the MLCK-independent component were modeled from ZO-1 FRAP curves of PIK-treated monolayers (Fig. S7*A* and Tables S2 and S4). The difference between recovery of control and PIK-treated monolayers was used to derive rate constants and pool size of the MLCK-dependent component of ZO-1 exchange. This approach showed that the MLCK-dependent process proceeded with slower kinetics than the MLCK-independent process (Fig. 5, Fig. S7, and Tables S2 and S4). Using the applied constants and initial pool sizes, the system was allowed to reach steady-state. As

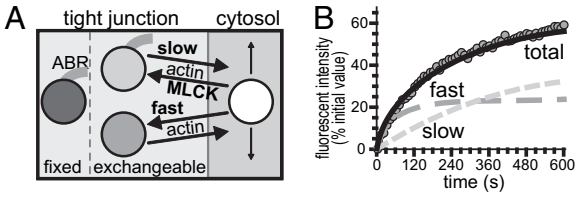

Fig. 5. In silico models of ZO-1 exchange. (*A*) ZO-1 was distributed in one cytosolic and three tight junction-associated pools. (*B*) Representative data showing in vitro ZO-1 FRAP (circles) in control monolayers and in silico models of total recovery (black line) as the sum of slow and fast components of recovery.

expected, subsequent activation of the virtual laser resulted in overall ZO-1 FRAP kinetics identical to those observed in vitro (Fig. 5*B* and Fig. S7*A*).

In silico inhibition of the MLCK-dependent process (without any additional changes to the model) reduced the mobile fraction of recovery to match that of monolayers treated with PIK in vitro (Fig. S7*B* and Tables S2 and S4). In silico inhibition of MLCK-dependent exchange also accelerated recovery, i.e., reduced the $t_{1/2}$ in a manner similar to that observed in vitro. The model demonstrates that overall $t_{1/2}$ is a weighted average of the slow and fast pathways, thereby explaining why complete inhibition of the slow pathway, which leaves only fast exchange, results in an overall reduction of $t_{1/2}$ despite a reduced mobile-fraction.

The in vitro data show that the mobile fraction of ZO-$1^{\Delta ABR}$ was greater than that of ZO-1. The ABR therefore contributes to ZO-1 stabilization at the tight junction. The validity of this conclusion was tested in silico by reducing the size of the fixed pool without making any other changes. This small modification reproduced the in vitro results (Fig. S7*C* and Tables S2 and S4). Moreover, because this was possible without altering exchange rates, the data support the hypothesis that the primary role of the ABR is to stabilize tight junction-associated ZO-1 rather than regulate transport of ZO-1 between the tight junction and cytosol.

The transport processes responsible for ZO-1 and ZO-$1^{\Delta ABR}$ exchange are energy dependent (Fig. S5) and are, therefore, likely to be saturable. It follows that the size of the exchangeable pool is limited by the capacity of the transport process. If, as suggested above, the ABR stabilizes ZO-1 but does not play a role in transport, full-length ZO-1 and ZO-$1^{\Delta ABR}$ should compete equally for transport. ZO-$1^{\Delta ABR}$ expression should therefore reduce the absolute number of full-length ZO-1 molecules in the exchangeable pool (ZO-$1^{FL}{}_e$). However, the absolute number of full-length ZO-1 molecules in the fixed pool (ZO-$1^{FL}{}_f$) should be reduced to a lesser extent, as ZO-$1^{\Delta ABR}$ is not stabilized via the ABR-dependent mechanism and cannot compete for those binding sites. Thus, ZO-$1^{\Delta ABR}$ expression is expected to cause a greater reduction in ZO-$1^{FL}{}_e$ than in ZO-$1^{FL}{}_f$, and the full-length ZO-1 mobile fraction (ZO-$1^{FL}{}_{Mf}$), ZO-$1^{FL}{}_{Mf}$ = ZO-$1^{FL}{}_e$/(ZO-$1^{FL}{}_e$ + ZO-$1^{FL}{}_f$), will be reduced. This was the in vitro result (Fig. S6*D*).

The in vitro data indicate that exchange of both tight junction-associated ZO-1 pools requires intact actomyosin function. The effects of latrunculin A were therefore modeled by reducing rate constants for both mechanisms. This reproduced the in vitro data (Fig. S7*D* and Table S2 and S4). This model also predicted that extended treatment with latrunculin A would result in progressive ZO-1 loss from the tight junction, consistent with previous reports of ZO-1 loss after prolonged actin disruption (10, 23). Thus, a mathematical model developed from experimental data can be rationally modified to recapitulate targeted interventions.

To assess the applicability of this in silico model to the vivo data, small adjustments to rate constants and initial pool sizes were made to reflect the slightly greater mobile fraction and shorter $t_{1/2}$ observed in vivo (Figs. S2*F* and S8 *A* and *B* and Tables S2 and S3). Because ZO-1 FRAP of long $MLCK^{-/-}$ mice without or with PIK treatment was similar to wild-type mice (without PIK), the parameters developed for wild-type mice were used to model long $MLCK^{-/-}$ mice (Fig. S8 *C* and *D* and Table S5).

The effect of MLCK activation was tested by assessing the effect of increasing the in silico rate of exchange via the slow, but not the fast, pathway. Changes to the model were limited to acceleration of this reaction. This single modification accurately modeled the in vivo data by reducing the $t_{1/2}$ of recovery without significantly affecting the ZO-1 mobile fraction (Fig. S8*E* and Tables S3 and S5). Moreover, the overall size of the tight junction-associated ZO-1 pool was not affected, consistent with the distribution of ZO-1 in CA-MLCK transgenic mice (7). Because CA-MLCK and MLCK are both inhibited by PIK (6, 7), ZO-1 FRAP in PIK-treated CA-MLCK transgenic mice was modeled by blocking exchange via the slow pathway (Fig. S8*F* and Tables S3 and S5), and this reproduced the in vivo results. As a whole, these data show that biology-based adjustments to a single model can explain ZO-1 and ZO-$1^{\Delta ABR}$ exchange in vitro and in vivo under a variety of experimental conditions as well as in genetically-modified animals.

Discussion

An essential role for MLCK in tight junction barrier regulation has been demonstrated in response to physiological and pathophysiological tight junction barrier regulation using in vitro and in vivo models (10–12, 19). Although light and electron microscopic analyses have associated MLCK activation with subtle changes in perijunctional actomyosin ring structure, tight junction morphology, and ZO-1 distribution (10, 19, 24), the molecular events responsible for MLCK-dependent barrier regulation have been elusive. Based on the recent observation that protein components of the tight junction are highly dynamic at steady-state (3), we asked if the molecular interactions responsible for dynamic protein behavior might be altered by MLCK-dependent barrier regulation. We also hypothesized that changes in dynamic protein behavior might be responsible for the barrier regulation observed.

Under basal conditions, when MLCK is active (11), steady-state exchange of tight junction-associated claudin-1, occludin, ZO-1, and actin in Caco-2 monolayers was comparable to that reported previously in MDCK cells (3). MLCK inhibition only affected exchange of ZO-1, which was profoundly reduced. Tight junction-associated ZO-1 was similarly stabilized following in vivo MLCK inhibition. Consistent with a role for MLCK in regulation of ZO-1 exchange, recovery was accelerated by in vivo MLCK activation. In vitro analyses demonstrated that the ABR was required for ZO-1 stabilization after MLCK inhibition, but that ZO-$1^{\Delta ABR}$ exchange remained sensitive to functional actomyosin disruption. This suggests that ZO-1 FRAP occurs by at least two mechanisms that can be differentiated by the critical role of the ABR in MLCK-dependent exchange for one, but not the other, but that both mechanisms of exchange require intact actomyosin function.

To better define the role of the ABR, we stably expressed this domain as an EGFP fusion protein. This reduced tight junction barrier function in a manner that required the presence of endogenous ZO-1, suggesting that the free ABR was able to interfere specifically with ZO-1 function. Consistent with this, ABR expression suppressed basal ZO-1 exchange and also blocked ZO-1 stabilization following MLCK inhibition. Moreover, interfering with ZO-1 stabilization, either by ZO-1 knockdown or ABR expression, prevented barrier function increases after MLCK inhibition. Thus, ZO-1 interactions mediated by the ABR are critical to MLCK-dependent barrier regulation.

To understand the process of ZO-1 exchange, we modeled the in vitro and in vivo data in silico. A previous analysis modeled ZO-1

as a cytosolic pool and two tight junction-associated pools, one exchangeable and one fixed (3). However, the results obtained here suggest that at least two exchangeable pools of ZO-1 must exist at the tight junction and that these must be differentially regulated. One pathway requires MLCK activity, and ZO-1 within this pool, as well as the nonexchangeable pool, is stabilized by ABR-mediated interactions. In contrast, neither the ABR nor MLCK affect the rapidly-exchangeable pool. Exchange of both pools requires actomyosin function. Based on this simple model (Fig. 5) and logical modifications of either the size of the ZO-1 fixed pool or the rate of MLCK-dependent ZO-1 exchange (but not both), we were able to completely recapitulate the in vitro and in vivo data. Although these results do not prove that the model is correct, they are consistent with that hypothesis and will serve as an important basis for further investigation of the roles of molecular dynamics in tight junction regulation. The data also suggest that ABR-mediated stabilization of tight junction-associated ZO-1 is critical to barrier regulation by MLCK.

Interestingly, ours is not the first study showing that loss of ZO-1 expression does not markedly affect TER (25–27). This suggests that other proteins, for example ZO-2, may compensate for ZO-1 loss (25). Together with previous studies showing increased flux of large solutes following MLCK activation (19), our identification of a specific role for ZO-1 in MLCK-dependent barrier regulation suggests that ZO-1 interactions with the cytoskeleton regulate flux of large solutes via a tight junction leak pathway. Consistent with this, ZO-1 knockdown has been shown to increase large solute flux across the tight junction (26, 27), and a recent report demonstrated enhanced sensitivity of ZO-1 knockdown monolayers to cytochalasin D or calcium chelation (27). In contrast, the TER increase induced by rho kinase inhibition in control monolayers did not occur in ZO-1-knockdown MDCK monolayers (27). Thus, previous data, as well as the data presented here, indicate that ZO-1 is essential for cytoskeletally-mediated barrier regulation. Our data further demonstrate that MLCK and the ABR are central to this process and suggest that ZO-1 exchange and anchoring regulated by these elements are critical intermediates in barrier regulation.

Overall, these data provide evidence that the dynamic behavior of specific tight junction protein components is crucial to barrier regulation. Moreover, the in silico model suggests that small changes in rates of exchange reactions can have profound effects on tight junction structure and function. Ongoing characterization of these processes, including the structural domains and machinery that coordinate transport of tight junction components, may lead to detailed understanding of the molecular anatomy of the tight junction as well as the interactions that dictate barrier function.

Methods

In Vitro FRAP. Caco-2_{BBe} cells were grown on Transwell supports (Corning) and TER measured as described (11). Stable transfectants were developed as described (10, 11) with conservative substitutions, to evade shRNA, as necessary. FRAP was performed on a DM4000 microscope (Leica) equipped with a MicroPoint Laser System (Photonic Instruments), Leica 63× UVI objective, and 37-°C heated stage controlled by MetaMorph 7 (MDS). A region of interest was bleached with a nanosecond laser pulse using low intensities and <1-s exposures to minimize phototoxicity. MetaMorph 7 was used for analysis, as described (3).

In Vivo FRAP. Mice were developed and in vivo imaging performed as described (28) using an SP5 microscope (Leica) with a 40× NA 0.8 water immersion objective. mRFP1-ZO-1 was excited and bleached using the DPSS 561 laser. Analysis was as above.

In Silico Modeling. A model was created using Virtual Cell (3). Cells were modeled as cylinders with diameter of 30 μm and height of 10 μm with a 1-μm thick tight junction band. A 10 min equilibration preceded virtual laser activation to model the 15-min drug preincubation used in vitro and in vivo as 5 min of diffusion and 10 min of activity. The models used in this paper are accessible at the Virtual Cell web site vcell.org/vcell_models/published_models.html.

Statistics. Data are presented as mean ± SEM of at least three independent experiments with three or more replicates and analyzed by two-tailed Student's *t* test, with $P < 0.05$ considered significant.

ACKNOWLEDGMENTS. We thank J. M. Anderson and A. S. Fanning for ZO-1 constructs and S. Nalle, B. Umans, and A. J. M. Watson for critical review. This work was supported by National Institutes of Health Grants R01DK61931, R01DK68271, P01DK67887, T32HL007237, F32DK082134, P30CA14599, UL1RR024999 and a fellowship from the Crohn's and Colitis Foundation of America sponsored by L. M. Hoffman. The Virtual Cell is supported by NIH Grant Number P41RR013186 from the National Center For Research Resources.

1. Fanning AS, Anderson JM (2009) Zonula occludens-1 and -2 are cytosolic scaffolds that regulate the assembly of cellular junctions. *Ann N Y Acad Sci* 1165:113–120.
2. Sasaki H, et al. (2003) Dynamic behavior of paired claudin strands within apposing plasma membranes. *Proc Natl Acad Sci USA* 100:3971–3976.
3. Shen L, Weber CR, Turner JR (2008) The tight junction protein complex undergoes rapid and continuous molecular remodeling at steady state. *J Cell Biol* 181:683–695.
4. Capaldo CT, Macara IG (2007) Depletion of E-cadherin disrupts establishment but not maintenance of cell junctions in Madin-Darby canine kidney epithelial cells. *Mol Biol Cell* 18:189–200.
5. Madara JL, Pappenheimer JR (1987) Structural basis for physiological regulation of paracellular pathways in intestinal epithelia. *J Membr Biol* 100:149–164.
6. Shen L, et al. (2006) Myosin light chain phosphorylation regulates barrier function by remodeling tight junction structure. *J Cell Sci* 119:2095–2106.
7. Su L, et al. (2009) Targeted epithelial tight junction dysfunction causes immune activation and contributes to development of experimental colitis. *Gastroenterology* 136:551–563.
8. Nusrat A, Turner JR, Madara JL (2000) Molecular physiology and pathophysiology of tight junctions. IV. Regulation of tight junctions by extracellular stimuli: Nutrients, cytokines, and immune cells. *Am J Physiol Gastrointest Liver Physiol* 279:G851–G857.
9. Fanning AS, Ma TY, Anderson JM (2002) Isolation and functional characterization of the actin binding region in the tight junction protein ZO-1. *FASEB J* 16:1835–1837.
10. Shen L, Turner JR (2005) Actin depolymerization disrupts tight junctions via caveolae-mediated endocytosis. *Mol Biol Cell* 16:3919–3936.
11. Turner JR, et al. (1997) Physiological regulation of epithelial tight junctions is associated with myosin light-chain phosphorylation. *Am J Physiol* 273:C1378–C1385.
12. Zolotarevsky Y, et al. (2002) A membrane-permeant peptide that inhibits MLC kinase restores barrier function in in vitro models of intestinal disease. *Gastroenterology* 123:163–172.
13. Spector I, Shochet NR, Kashman Y, Groweiss A (1983) Latrunculins: Novel marine toxins that disrupt microfilament organization in cultured cells. *Science* 219:493–495.
14. Coué M, Brenner SL, Spector I, Korn ED (1987) Inhibition of actin polymerization by latrunculin A. *FEBS Lett* 213:316–318.
15. Bubb MR, Senderowicz AM, Sausville EA, Duncan KL, Korn ED (1994) Jasplakinolide, a cytotoxic natural product, induces actin polymerization and competitively inhibits the binding of phalloidin to F-actin. *J Biol Chem* 269:14869–14871.
16. Allingham JS, Smith R, Rayment I (2005) The structural basis of blebbistatin inhibition and specificity for myosin II. *Nat Struct Mol Biol* 12:378–379.
17. Straight AF, et al. (2003) Dissecting temporal and spatial control of cytokinesis with a myosin II Inhibitor. *Science* 299:1743–1747.
18. Just I, et al. (1995) Glucosylation of Rho proteins by Clostridium difficile toxin B. *Nature* 375:500–503.
19. Clayburgh DR, et al. (2005) Epithelial myosin light chain kinase-dependent barrier dysfunction mediates T cell activation-induced diarrhea in vivo. *J Clin Invest* 115:2702–2715.
20. Clayburgh DR, et al. (2004) A differentiation-dependent splice variant of myosin light chain kinase, MLCK1, regulates epithelial tight junction permeability. *J Biol Chem* 279: 55506–55513.
21. Fanning AS, Jameson BJ, Jesaitis LA, Anderson JM (1998) The tight junction protein ZO-1 establishes a link between the transmembrane protein occludin and the actin cytoskeleton. *J Biol Chem* 273:29745–29753.
22. Turner JR (2000) 'Putting the squeeze' on the tight junction: Understanding cytoskeletal regulation. *Semin Cell Dev Biol* 11:301–308.
23. Stevenson BR, Begg DA (1994) Concentration-dependent effects of cytochalasin D on tight junctions and actin filaments in MDCK epithelial cells. *J Cell Sci* 107:367–375.
24. Madara JL, Carlson S, Anderson JM (1993) ZO-1 maintains its spatial distribution but dissociates from junctional fibrils during tight junction regulation. *Am J Physiol* 264: C1096–C1101.
25. Umeda K, et al. (2006) ZO-1 and ZO-2 independently determine where claudins are polymerized in tight-junction strand formation. *Cell* 126:741–754.
26. Umeda K, et al. (2004) Establishment and characterization of cultured epithelial cells lacking expression of ZO-1. *J Biol Chem* 279:44785–44794.
27. Van Itallie CM, Fanning AS, Bridges A, Anderson JM (2009) ZO-1 stabilizes the tight junction solute barrier through coupling to the perijunctional cytoskeleton. *Mol Biol Cell* 20:3930–3940.
28. Marchiando AM, et al. (2010) Caveolin-1-dependent occludin endocytosis is required for TNF-induced tight junction regulation in vivo. *J Cell Biol* 188:111–126.

Supporting Information

Yu et al. 10.1073/pnas.0908869107

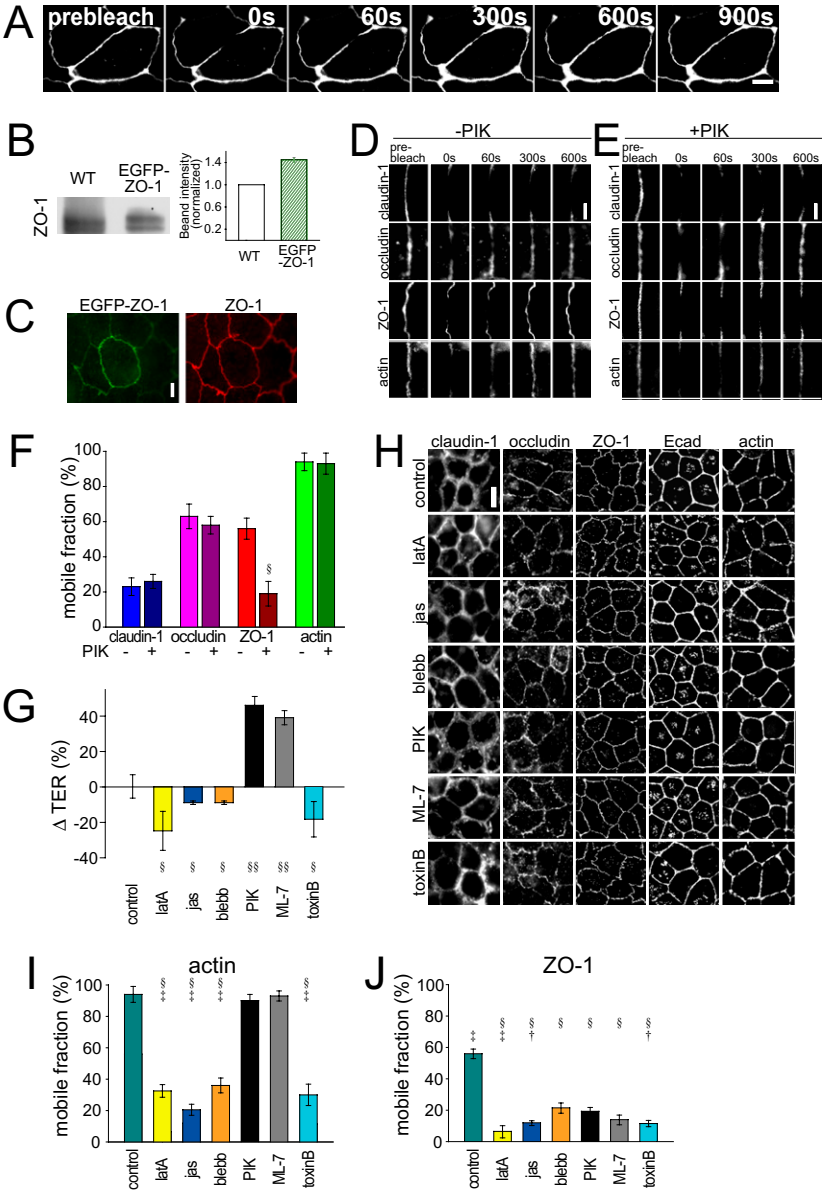

Fig. S1. ZO-1 exchange is uniquely sensitive to MLCK inhibition in vitro. (*A*) Representative FRAP experiment assessing recovery of tight junction-associated EGFP-ZO-1. (Scale bar, 3 μm.) (*B*) Western blot of endogenous and EGFP-tagged ZO-1 in wild-type and EGFP-ZO-1-transfected Caco-2. Densitometry shows that transfection induced a 40% increase in total ZO-1 expression, $n = 2$ per condition. (*C*) EGFP-ZO-1-transfected Caco-2 cells were fixed and stained for endogenous ZO-1. Although EGFP-ZO-1 expression is heterogeneous, total ZO-1 expression is uniform. This indicates that expression of EGFP-ZO-1 did not markedly alter overall ZO-1 expression. (Scale bar, 3 μm.) (*D*) FRAP experiments were performed on Caco-2 monolayers stably expressing fluorescent fusion constructs of the indicated proteins. Images of the tight junction before and at the indicated time points after photobleaching corresponding to the kymographs in Fig. 1 are shown. (Scale bar, 3 μm.) (*E*) FRAP experiments were performed 15 min after addition of the specific MLCK inhibitor PIK (250 μM). (Scale bar, 3 μm.) (*F*) Mobile fractions of indicated proteins were determined in the absence or presence of PIK treatment, $n = 3$ per condition. § $P < 0.001$ vs. same protein without PIK. (*G*) TER of monolayers was determined 15 min after addition of 0.5 μM latrunculin A (latA); 1 μM jasplakinolide (jas); 10 μM blebbistatin (blebb); 250 μM PIK; 10 μM ML-7; or 40 ng/mL toxin B, $n = 3$ per condition. § $P < 0.05$ vs. vehicle control. §§ $P < 0.01$ vs. vehicle control. (*H*) Monolayers were fixed 15 min after addition of drugs, as in *G*. Indicated proteins were labeled by immunofluorescence. Overall distribution of these proteins was not grossly affected by drug treatments. (Scale bar, 10 μm.) (*I*) Mobile fraction of tight junction-associated EGFP-actin was assessed in monolayers 15 min after addition of drugs, $n = 4$ per condition. § $P < 0.01$ vs. vehicle control. † $P < 0.05$ vs. PIK-treated monolayers. ‡ $P < 0.01$ vs. PIK-treated monolayers. (*J*) Mobile fraction of EGFP-ZO-1 was assessed in monolayers 15 min after addition of drugs, $n = 4$ per condition. § $P < 0.01$ vs. vehicle control. † $P < 0.05$ vs. PIK-treated monolayers. $n = 4$. ‡ $P < 0.01$ vs. PIK-treated monolayers.

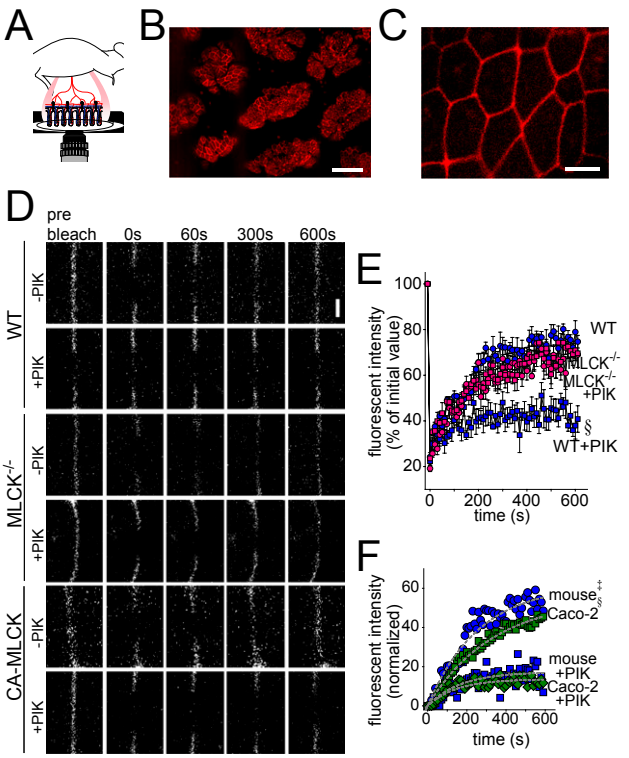

Fig. S2. In vivo ZO-1 FRAP is similar to that observed in vitro. (*A*) In vivo imaging was performed on neurovascularly-intact jejunum of anesthetized mice. (*B*) Low magnification images of jejunal villi of mRFP1-ZO1 transgenic mice. (Scale bar, 30 μm.) (*C*) High magnification images of jejunal epithelial cells expressing mRFP1-ZO-1. (Scale bar, 3 μm.) (*D*) FRAP experiments were performed in vivo on wild-type (WT), long MLCK$^{-/-}$, and CA-MLCK transgenic mice, all expressing mRFP1-ZO-1, before and after treatment with PIK (250 μM, 15 min). Images of the tight junction before and at the indicated time points after photobleaching corresponding to the kymographs in Fig. 2*A* are shown. (Scale bar, 3 μm.) (*E*) Mean recovery curves, $n = 5$ per condition. § $P < 0.001$ vs. wild type without PIK. (*F*) Comparison of in vivo (mouse) and in vitro (Caco-2) ZO-1 recovery curves in the absence or presence of PIK, $n = 5$ per condition in vivo, $n = 4$ per condition in vitro. § $P < 0.01$ vs. PIK-treated monolayers. ‡ $P < 0.001$ vs. PIK-treated mucosa.

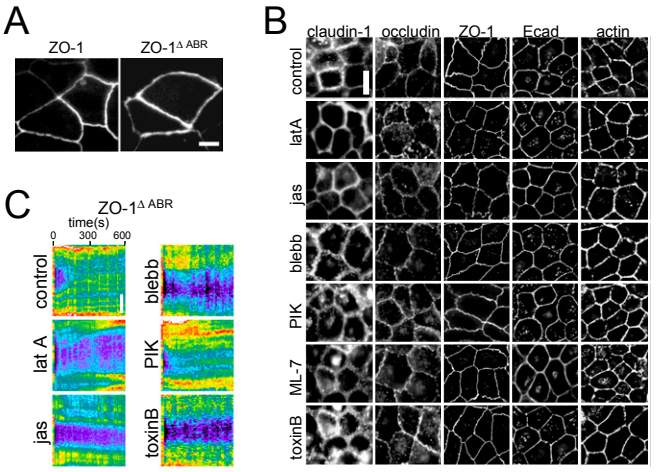

Fig. S3. ZO-1$^{\Delta ABR}$ exchange is resistant to myosin light chain kinase inhibition in vitro. (*A*) EGFP-tagged ZO-1 and ZO-1$^{\Delta ABR}$ concentrate at the tight junction of Caco-2 monolayers. (Scale bar, 3 μm.) (*B*) EGFP-ZO-1$^{\Delta ABR}$-expressing monolayers were fixed 15 min after addition of drugs, as in *C*. Indicated proteins were labeled by immunofluorescence. Overall distribution of these proteins was not grossly affected by EGFP-ZO-1$^{\Delta ABR}$ expression or drug treatments. (Scale bar, 10 μm.) (*C*) FRAP of EGFP-ZO-1$^{\Delta ABR}$ was assessed 15 min after addition of 0.5 μM latrunculin A (latA); 1μM jasplakinolide (jas); 10 μM blebbistatin (blebb); 250 μM PIK; 10 μM ML-7; or 40 ng/mL toxin B. Representative kymographs corresponding to the data in Fig. 3*B* are shown. (Scale bar, 3 μm.)

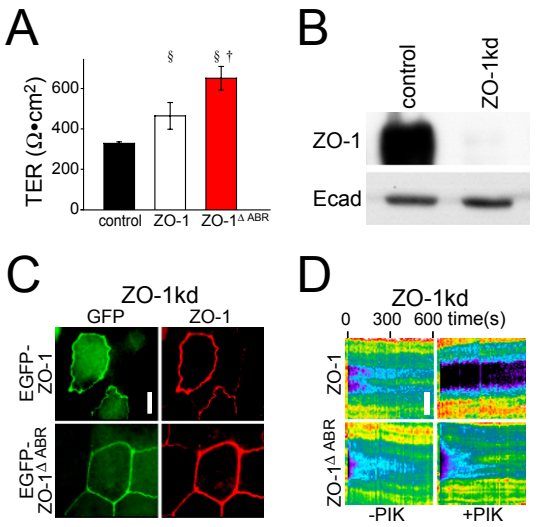

Fig. S4. Endogenous ZO-1 does not affect FRAP behavior of EGFP-ZO-1 or EGFP-ZO-1$^{\Delta ABR}$. (*A*) TER of nontransfected (wild-type) Caco-2 monolayers and cells stably transfected with EGFP-ZO-1 or EGFP-ZO-1$^{\Delta ABR}$, $n = 7$ per condition. § $P < 0.01$ vs. wild-type monolayers. † $P < 0.05$ vs. EGFP-ZO-1-expressing monolayers. EGFP-ZO-1 constructs were generated as reported (1, 2). (*B*) Stable ZO-1 knockdown lines were developed by cloning human ZO-1 targeting sequences into pSUPER. Multiple clones using the target sequence 5′-GATCAAATTCTCAGGGTAA-3′ showed >90% suppression of ZO-1 expression. The targeting sequence 5′-GCAAAGACATTGATAGGAA-3′ failed to inhibit ZO-1 expression, and these clones were used as controls. Western blot of ZO-1 knockdown (ZO-1kd) and corresponding control Caco-2 monolayers show that >95% of ZO-1 expression is suppressed. E-cadherin is shown as a loading control. (*C*) ZO-1 knockdown Caco-2 cells were transiently transfected with EGFP-ZO-1 or EGFP-ZO-1$^{\Delta ABR}$ constructs with conservative nucleotide sequence changes to escape shRNA knockdown. Confluent monolayers of these cells were fixed and immunostained to label ZO-1 (red). Note the absence of endogenous ZO-1 in adjacent cells that do not express transfected EGFP-tagged ZO-1 or ZO-1$^{\Delta ABR}$. (Scale bar, 5 μm.) (*D*) FRAP of EGFP–ZO-1 or EGFP-ZO-1$^{\Delta ABR}$ was assessed in ZO-1 knockdown cells before or 15 min after treatment with PIK (250 μM). (Scale bar, 5 μm.) See Fig. 3*B* for analysis.

1. Shen L, Weber CR, Turner JR (2008) The tight junction protein complex undergoes rapid and continuous molecular remodeling at steady state. *J Cell Biol* 181:683–695.
2. Fanning AS, Ma TY, Anderson JM (2002) Isolation and functional characterization of the actin binding region in the tight junction protein ZO-1. *FASEB J* 16:1835–1837.

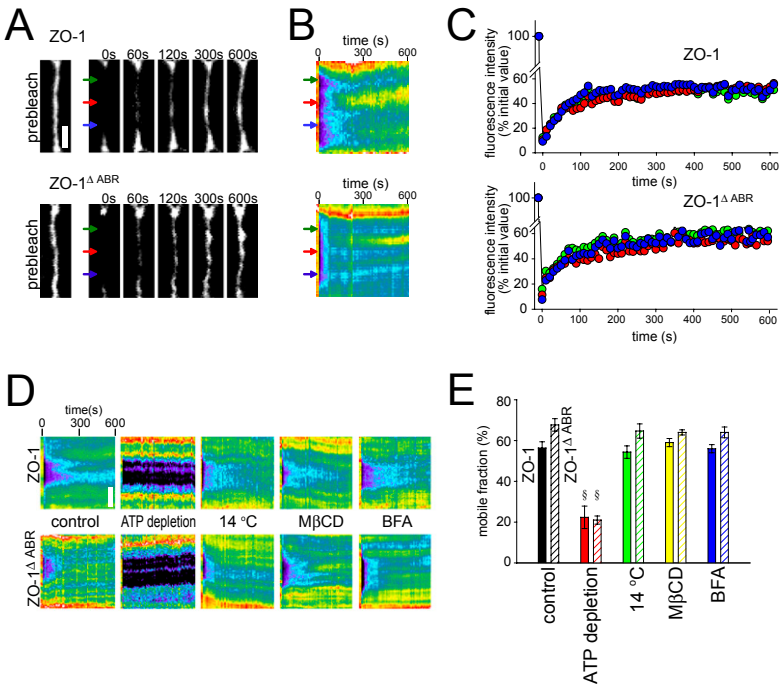

Fig. S5. Diffusion within the membrane does not contribute to FRAP of tight junction-associated ZO-1 or ZO-1$^{\Delta ABR}$. (*A*) EGFP–ZO-1 or EGFP-ZO-1$^{\Delta ABR}$ expressing cells within confluent monolayers were studied by FRAP after photobleaching elongated tight junction regions. Representative images before and at the indicated times after photobleaching are shown. (Scale bar, 3 μm.) (*B*) Kymographs corresponding to the images in *A*. (*C*) Recovery curves of indicated points were shown. (*D*) FRAP experiments were performed on EGFP–ZO-1 or EGFP-ZO-1$^{\Delta ABR}$ expressing cells within confluent monolayers after ATP depletion (by treatment for 60 min with 2 mM 2-D-deoxy-glucose, 1 mM 2,4-dinitrophenol, and 10 mM NaN_3 in glucose-free HBSS), chilling to 14 °C, treatment with 5 mM methyl β-cyclodextrin (MβCD) for 30 min, or treatment with 5 μM brefeldin A (BFA) for 30 min. Representative kymographs are shown. (Scale bar, 3 μm.) (*E*) Mobile fraction of EGFP–ZO-1 or EGFP-ZO-1$^{\Delta ABR}$ was determined, $n = 3$ per condition. § $P < 0.001$ vs. corresponding control monolayers.

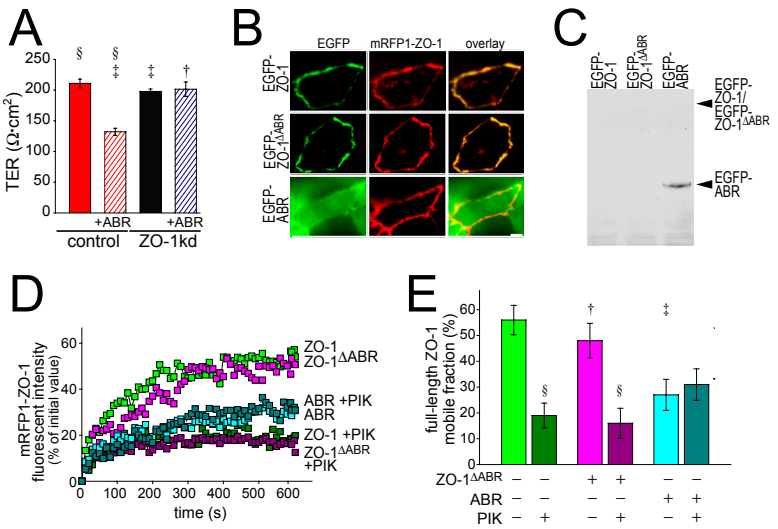

Fig. S6. EGFP-ABR inhibits ZO-1 exchange at the tight junction. (*A*) TER of control and ZO-1 knockdown (ZO-1kd) monolayers with or without EGFP-ABR expression, $n = 3$ per condition. § $P < 0.001$ vs. ZO-1 knockdown monolayers. † $P < 0.05$ vs. control monolayers. ‡ $P < 0.001$ vs. control monolayers. (*B*) Live images of monolayers expressing mRFP1-ZO-1 as well as EGFP-ZO-1, EGFP-ZO-1$^{\Delta ABR}$, or EGFP-ABR. (Scale bar, 3 μm.) (*C*) Western blot of EGFP-tagged proteins in Caco-2 cells stably transfected to express EGFP-ZO-1, EGFP-ZO-1$^{\Delta ABR}$, or EGFP-ABR. Whereas EGFP-ABR is easily seen, the limited expression of EGFP-ZO-1 and EGFP-ZO-1$^{\Delta ABR}$ (as shown in *A*) is below the level of detection. (*D*) Mean recovery curves for mRFP1-ZO-1 FRAP in monolayers also expressing EGFP-ZO-1, EGFP-ZO-1$^{\Delta ABR}$ or EGFP-ABR, as indicated, before or 15 min after addition of 250 μM PIK. (*E*) Mobile fraction of mRFP1–ZO-1 was determined for the conditions in *D*. $n = 3$. § $P < 0.001$ vs. corresponding untreated monolayers. † $P < 0.05$ vs. full-length EGFP-ZO-1-expressing cells. ‡ $P < 0.01$ vs. full-length EGFP-ZO-1-expressing cells.

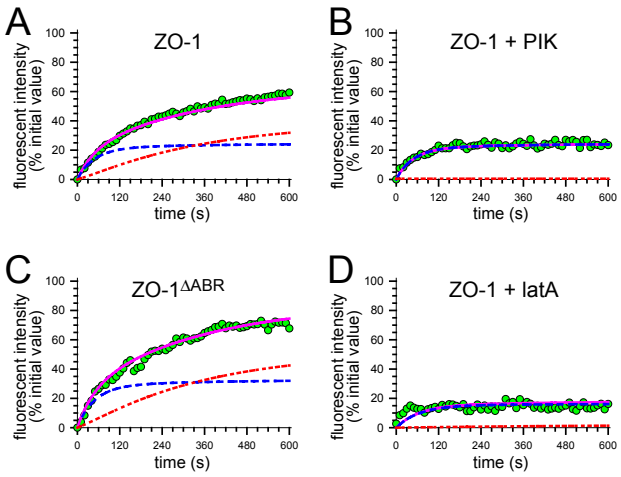

Fig. S7. In vitro and in silico analyses of ZO-1 FRAP. The model (Fig. 5 and Tables S2 and S4) was used to calculate in silico FRAP behavior. Total in silico recovery (purple lines) is the sum of the slow (red lines) and fast (blue lines) components. This is compared to in vitro data (green circles). (*A*) ZO-1 recovery in control monolayers. (*B*) ZO-1 recovery in PIK-treated monolayers. The model after ML-7 treatment was similar. (*C*) ZO-1$^{\Delta ABR}$ recovery in control monolayers. As MLCK inhibition did not affect ZO-1$^{\Delta ABR}$ exchange, the model was identical after PIK treatment. (*D*) ZO-1 recovery in latrunculin A-treated (latA) monolayers. Models of jasplakinolide, toxin B, and blebbistatin treatment effects were similar.

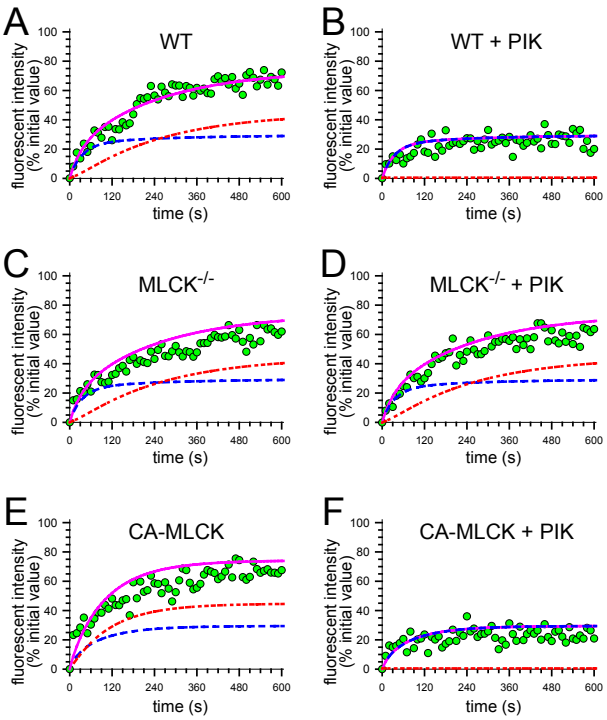

Fig. S8. In vivo and in silico analyses of ZO-1 FRAP. The model (Fig. 5 and Tables S3 and S5) was used to calculate in silico FRAP behavior. Total in silico recovery (purple lines) is the sum of the slow (red lines) and fast (blue lines) components. This is compared to in vivo data (green circles). (*A*) ZO-1 recovery in mucosa of untreated wild-type mice. (*B*) ZO-1 recovery in mucosa of PIK-treated wild-type mice. (*C*) ZO-1 recovery in mucosa of untreated long MLCK$^{-/-}$ mice. (*D*) ZO-1 recovery in mucosa of PIK-treated long MLCK$^{-/-}$ mice. (*E*) ZO-1 recovery in mucosa of untreated CA-MLCK mice. (*D*) ZO-1 recovery in mucosa of PIK-treated CA-MLCK mice.

Table S1. In vitro analysis of tight junction protein dynamics: Comparison of in vitro protein exchange in MDCK and Caco-2 monolayers

	Protein studied			
	claudin-1	occludin	ZO–1	actin
Caco-2 fraction (%)	24 ± 5	63 ± 3	56 ± 3	94 ± 3
MDCK mobile fraction* (%)	22 ± 2	77 ± 3	73 ± 3	97 ± 3
Caco-2 $t_{1/2}$ (s)	158 ± 14	79 ± 6	125 ± 8	46 ± 7
MDCK $t_{1/2}$* (s)	195 ± 65	107 ± 8	98 ± 16	43 ± 8

*Results from MDCK monolayers 10 days after confluence (1).

1. Shen L, Weber CR, Turner JR (2008) The tight junction protein complex undergoes rapid and continuous molecular remodeling at steady state. *J Cell Biol* 181:683–695.

Table S2. In vitro and in silico analysis of tight junction protein dynamics: Comparison of ZO-1 exchange in vitro and in silico

	Protein studied			
	ZO-1	ZO-1 with PIK treatment	ZO–1$^{\Delta ABR}$	ZO-1 with latA treatment
In vitro mobile fraction	56 ± 3	20 ± 5*	81 ± 5*	14 ± 6*
In silico mobile fraction	55	24	73	17
In vitro $t_{1/2}$ (s)	125 ± 8	39 ± 11*	105 ± 6	13 ± 6*
In silico $t_{1/2}$ (s)	110	41	110	52

*$P < 0.001$ vs. ZO-1 (without drugs).

Table S3. In vivo and in silico analysis of ZO-1 dynamics: Comparison of ZO-1 exchange in vivo and in silico

	Genotype					
	Wild type		Long MLCK$^{-/-}$		CA-MLCK	
Treatment	−PIK	+PIK	−PIK	+PIK	−PIK	+PIK
In vivo mobile fraction	70 ± 5	26 ± 4*	64 ± 7	62 ± 3	64 ± 3	25 ± 7*
In silico mobile fraction	68	28	68	68	73	28
In vivo $t_{1/2}$ (s)	97 ± 10	44 ± 9*	107 ± 20	113 ± 20	64 ± 7†	17 ± 8*
In silico $t_{1/2}$ (s)	98	32	98	98	67	32

*$P < 0.01$ vs. corresponding genotype without PIK.
$^{\dagger}P < 0.05$ vs. wild type under corresponding conditions.

Table S4. In silico analysis of tight junction protein dynamics: Parameters defining the model of in vitro ZO-1 FRAP behavior

	Protein studied			
	ZO-1	ZO-1 with PIK treatment	ZO−1$^{\Delta ABR}$	ZO-1 with latA treatment
TJ pool				
Slowly-exchangeable (slow) pool	21%	21%	24%	7%
Rapidly-exchangeable (fast) pool	13%	13%	15%	5%
Fixed (nonexchangeable) pool	18%	18%	6%	19%
Intracellular pool	48%	48%	55%	69%
TJ diffusion constant (all pools), um^{2}s^{-1}	0	0	0	0
Intracellular diffusion constant, um^{2}s^{-1}	1	1	1	1
Rate constant (movement to TJ), um^{2}s^{-1}				
Slowly-exchangeable (slow) pool	65	0	65	0.75
Rapidly-exchangeable (fast) pool	425	425	425	53
Fixed (nonexchangeable) pool	0	0	0	0
Rate constant (movement from TJ), s^{-1}				
Slowly-exchangeable (slow) pool	0.0033	0	0.0033	0.0019
Rapidly-exchangeable (fast) pool	0.034	0.034	0.034	0.017
Fixed (nonexchangeable) pool	0	0	0	0

Table S5. In silico analysis of ZO-1 dynamics: Parameters defining the model of in vivo ZO-1 FRAP behavior

	Genotype					
	Wild type		long MLCK$^{-/-}$		CA-MLCK	
Treatment	−PIK	+PIK	−PIK	+PIK	−PIK	+PIK
TJ pool						
Slowly-exchangeable (slow) pool	23%	23%	23%	23%	23%	23%
Rapidly-exchangeable (fast) pool	15%	15%	15%	15%	15%	15%
Fixed (nonexchangeable) pool	12%	12%	12%	12%	12%	12%
Intracellular pool	50%	50%	50%	50%	50%	50%
TJ diffusion constant (all pools), um^{2}s^{-1}	0	0	0	0	0	0
Intracellular diffusion constant, um^{2}s^{-1}	1	1	1	1	1	1
Rate constant (movement to TJ), um^{2}s^{-1}						
Slowly-exchangeable (slow) pool	100	0	100	100	400	0
Rapidly-exchangeable (fast) pool	850	850	850	850	850	850
Fixed (nonexchangeable) pool	0	0	0	0	0	0
Rate constant (movement from TJ), s^{-1}						
Slowly-exchangeable (slow) pool	0.005	0	0.005	0.005	0.02	0
Rapidly-exchangeable (fast) pool	0.06	0.06	0.06	0.06	0.06	0.06
Fixed (nonexchangeable) pool	0	0	0	0	0	0